Rare Metal Materials and Engineering
Volume 55, Issue 5, May 2026
Available online at www.rmme.ac.cn

Science Press

Cite this article as: Liu Xiaoyan, Wang Zixuan, Yang Xirong, et al. Low-Cycle Fatigue Behavior of Ultrafine-Grained Pure Titanium[J]. Rare Metal Materials and Engineering, 2026, 55(05): 1191-1198. DOI: https://doi.org/10.12442/j.issn.1002-185X.20250036.

ARTICLE

Low-Cycle Fatigue Behavior of Ultrafine-Grained Pure Titanium

Liu Xiaoyan, Wang Zixuan, Yang Xirong, Luo Lei, Wang Jingzhong

School of Metallurgical Engineering, Xi'an University of Architecture and Technology, Xi'an 710055, China

Abstract: Ultrafine-grained (UFG) pure titanium was produced by equal channel angular pressing for 4 passes, followed by rotatory swaging at room temperature. The strain-controlled low-cycle fatigue tests of UFG and coarse-grained (CG) pure titanium were conducted by Instron electro-hydraulic servo fatigue testing machine in the strain amplitude range of 0.5%–1.1% at room temperature. Transmission electron microscope (TEM) and scanning electron microscope were used to investigate the microstructure and fracture surface of UFG pure titanium after fatigue tests. Results show that UFG pure titanium exhibits a longer low-cycle fatigue life, compared with the CG pure titanium. For example, at a total strain amplitude of 0.5%, UFG and CG pure titanium has fatigue life of 10 850 and 4820 cycles, respectively. Significant cyclic softening occurs in UFG pure titanium, except in the case of a total strain amplitude of 0.5%. Hysteresis loop area is increased rapidly with the increase in strain amplitude. The fracture surface shows that the fatigue crack is initiated from the specimen surface. A series of fatigue striations and many microcracks exist in the propagation region. With the increase in strain amplitude, the predominant failure mode is transformed from ductile failure into quasi-cleavage failure. Dislocation slip is the main plastic deformation mechanism of UFG pure titanium during low-cycle fatigue deformation.

Key words: ultrafine-grained pure titanium; equal channel angular pressing+rotatory swaging; low-cycle fatigue; dislocation slip

1 Introduction

Titanium and its alloys are widely used in aerospace, shipbuilding, automobile, and biology fields due to their high strength, low modulus of elasticity, non-toxicity, good biocompatibility, and corrosion resistance[1–3]. However, the strength and fatigue behavior of conventional pure titanium are inferior, compared with other metallic alloys, such as TC4, which restricts its further application. Equal channel angular pressing (ECAP) is expected to be a critical method to improve the strength and fatigue resistance of metal materials by significant grain refinement. Ultrafine-grained (UFG) pure titanium with high mechanical properties but no biocompatibility degradation has been fabricated by ECAP[4–6].

Currently, the low-cycle fatigue (LCF) behavior and life of UFG materials have received considerable scientific attention. Generally, UFG materials prepared by ECAP exhibit shorter fatigue lives in LCF regime than their corresponding coarse-grained (or conventional-grained, CG) counterparts, because they have lower ductility[7–14]. LCF lives of UFG AA6061 and UFG Cu prepared by ECAP are significantly shorter than those of their CG counterparts. The fatigue life can be improved by appropriate heat treatment after ECAP due to the stabilization of UFG microstructure. However, this method does not suit UFG copper: LCF life remains shorter than that of its CG counterpart[7]. With higher plastic strain amplitude, UFG Ti-6Al-4V alloy shows deteriorated fatigue lives due to its reduced elongation, compared with that of its CG counterpart[8]. However, Ref.[12–14] reported contrary results. Under the same strain amplitude of 0.4%, the 6063 aluminum alloy processed by ECAP with dies of 90° and 120° has fatigue life of 7489 and 5860 cycles, respectively, whereas the Al6063-T6 alloy has fatigue life of 1286 cycles[12]. LCF properties of Fe-36Ni Invar alloy remain excellent after ECAP due to its good ductility[13].

At present, extensive research has been conducted on the

Received date: May 18, 2025
Foundation item: Natural Science Foundation of Shaanxi Province (2023-JC-YB-312)
Corresponding author: Liu Xiaoyan, Ph. D., Associate Professor, School of Metallurgical Engineering, Xi'an University of Architecture and Technology, Xi'an 710055, P. R. China, E-mail: liuxiaoyan@xauat.edu.cn

cycle deformation and fatigue life of UFG titanium. However, these studies have predominantly focused on high-cycle fatigue (HCF) conditions. The fatigue life and fatigue limit in HCF process of UFG titanium have been improved due to the microstructure refinement and higher tensile strength of UFG titanium, compared with its CG counterpart[9,15–18]. The enhancement in fatigue life and strength during stress-controlled tests, namely under HCF conditions, cannot ensure the improvement of cyclic properties in strain-controlled tests, namely under LCF conditions. Vinogradov et al[9] investigated the LCF behavior of UFG titanium prepared by ECAP at elevated temperatures. At high plastic strain amplitude of 0.5%, UFG titanium has longer fatigue life. While at low plastic strain amplitudes of 0.2% and 0.1%, UFG titanium has shorter fatigue life, compared with CG titanium. Using a combination of ECAP and subsequent thermal and mechanical treatments, it is possible to prolong the LCF life of UFG materials. The enhancement in LCF life by 2–4 times can be achieved for commercially pure zirconium processed by ECAP+rotary swaging (RS) at room temperature, which is primarily attributed to the refined grain structure (average grain size about 250 nm) and effective suppression of localized strain accumulation during cyclic deformation[14].

To gain an insight into the fatigue behavior and the possibility to optimize LCF life of UFG pure titanium at low strain amplitudes, it is necessary to use special methods, such as the combination of ECAP and subsequent additional deformation, to control the microstructures, including the shape and size of grains and grain boundaries with high-angle misorientation. Thus, the fatigue performance in low-cyclic regimes of UFG pure titanium produced by ECAP+RS at room temperature was investigated in this research. The cyclic response, evaluation of fatigue life, fatigue fracture, and deformation mechanisms were analyzed.

2 Experiment

The chemical composition (wt%) of the rods of pure titanium is Ti-0.2Fe-0.03N-0.08C-0.18O-0.015H. The billets with diameter of 25 mm and length of 200 mm were annealed at 650 °C for 1 h. Then, the billets were processed by ECAP for 4 passes at room temperature via route C (the rods were rotated at 180° in the same direction along their longitudinal axis between each pass) in a die-set with channels intersecting at an angle of 135°. ECAP billets were further processed by RS at room temperature to obtain specimens with 10 mm in diameter. After all these treatments, UFG pure titanium was prepared. Tensile tests were conducted at room temperature using a universal mechanical testing machine at strain rate of 10^{-3} s^{-1}. The gauge dimension of tensile specimens was Φ5 mm×25 mm. The tensile properties of CG and UFG pure titanium are listed in Table 1. It can be seen that the yield strength and ultimate tensile strength of UFG pure titanium are much higher than those of CG pure titanium. However, the elongation of UFG pure titanium is obviously lower than that of CG pure titanium.

LCF tests were conducted using an Instron electro-hydraulic servo fatigue testing machine with a triangular waveform at a frequency of 0.23 – 0.50 Hz at room temperature. Fully-reversed strain-controlled tests were conducted at total strain amplitude ranging from 0.5% to 1.1% at a strain ratio of $R=-1$. The specimens for LCF tests were machined along the UFG pure titanium billets, and the schematic diagram of fatigue specimen is shown in Fig. 1. For a comparative analysis, LCF tests of CG pure titanium were conducted under the same conditions.

Table 1 Tensile properties of CG and UFG pure titanium

Pure titanium	Yield strength/MPa	Ultimate tensile strength/MPa	Elongation/%
CG	191±2	338±2	55.5±2.5
UFG	756±2	788±3	14.5±1.0

The microstructure characterization of the specimens before and after fatigue was performed using optical microscope (OM) and transmission electron microscope (TEM, JEM-200CX, 200 kV). The thin foils for TEM observations were prepared by mechanically thinning followed by double jet polishing at 243 K in a mixed solution of 5 mL perchloric acid, 35 mL butanol, and 60 mL methanol. The fracture surfaces were observed by scanning electron microscope (SEM, FEI Q25).

3 Results and Discussion

3.1 Microstructure

Fig. 2 shows typical microstructures and selected area electron diffraction (SAED) pattern of CG and UFG pure titanium processed by ECAP+RS. It can be seen that CG pure titanium has an equiaxed α microstructure with an average grain size of about 27 μm (Fig. 2a). The equiaxed grains/subgrains can be clearly observed with a relatively high density of dislocations in UFG pure titanium (Fig. 2b). Most dislocations are distributed in the grain boundaries, and the grain interiors barely have dislocations. Fig. 2c indicates that there are a large number of grain boundaries with high angles of misorientation. The grains have an average size of approximately 200 nm, which is measured by the intercept method based on Fig. 2b. Some diffraction spots are split, demonstrating the existence of a small fraction of low-angle grain boundaries. The elongated diffraction spots in SAED pattern may demonstrate the high internal stress in the microstructure, which are commonly found in severe-plastic-deformation materials.

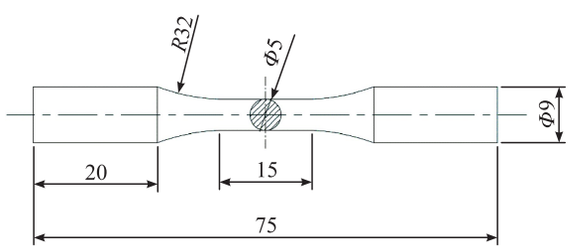

Fig.1 Schematic diagram of fatigue specimen

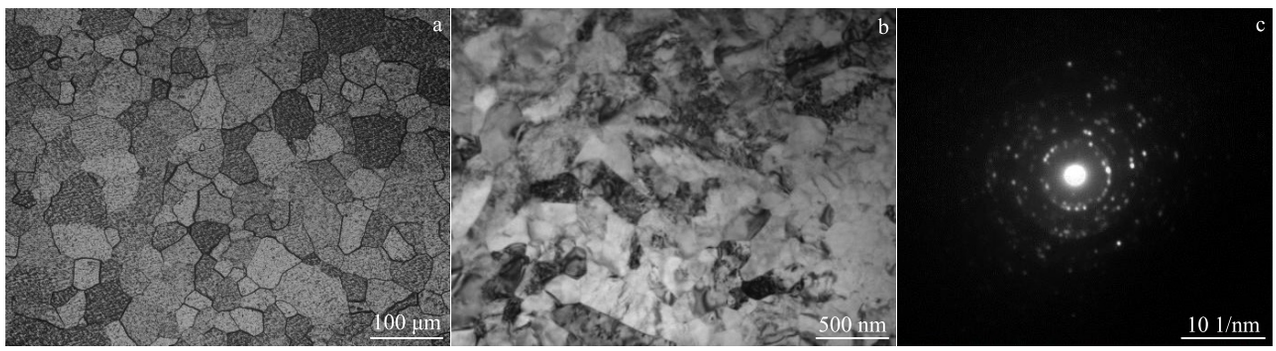

Fig.2 OM microstructure of CG pure titanium processed by ECAP+RS (a); TEM image (b) with SAED pattern (c) of UFG pure titanium processed by ECAP+RS

3.2 LCF behavior

To investigate the influence of total strain amplitudes on the hardening or softening behavior of UFG pure titanium, cyclic stress response curves under different strain amplitudes are shown in Fig. 3. UFG pure titanium exhibits the progressive cyclic strain softening from the beginning at high strain amplitude (0.6%–1.1%), whereas at low total strain amplitude of 0.5%, UFG pure titanium shows initial hardening followed by saturation till the end of testing. The softening effect becomes more obvious with the increase in strain amplitude, i. e., softening behavior is more severe and occurs earlier at strain amplitude of 1.1% than at strain amplitude of 0.6%. Similar cyclic softening results have been obtained on other UFG materials, such as Al alloy[10], Cu alloy[19], Ti alloy[9], and Mg alloy [20]. These results indicate a higher stability of ECAP-treated structure during the processing.

The cyclic stress-strain curve can be expressed by Eq.(1)[21]:

$$\frac{\Delta\sigma}{2} = K'\left(\frac{\Delta\varepsilon_p}{2}\right)^{n'} \quad (1)$$

where σ is stress, K' is a cyclic strength coefficient, $\Delta\varepsilon_p$ is plastic strain amplitude, and n' is a cyclic strain hardening exponent. The stress amplitude and the plastic strain amplitude in the formula correspond to the value of the half period. The data points in Fig. 4 are all obtained from cyclic hysteresis loops at half-life time. It can be seen that for UFG pure titanium, there is no linear relationship between stress and plastic strain. K' and n' can be determined according to

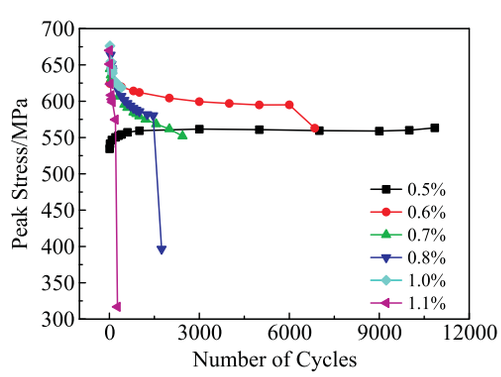

Fig.3 Cyclic stress response curves of UFG pure titanium under different strain amplitudes

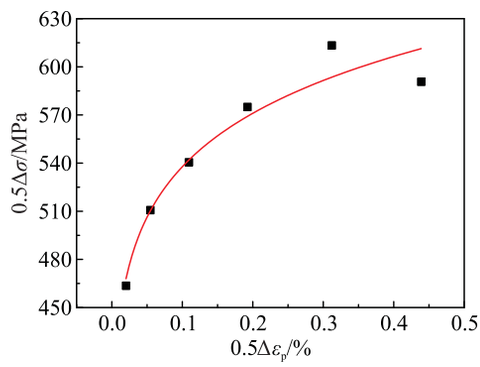

Fig.4 Relationship between $0.5\Delta\sigma$ and $0.5\Delta\varepsilon_p$ of UFG pure titanium

the fitting analysis of the experiment data in Fig.4 as 656.577 MPa and 0.086 72, respectively.

The hysteresis loops of UFG pure titanium at a half-life cycle under different total strain amplitudes are shown in Fig. 5. It can be seen that the tensile peak stress and compressive peak stress of the hysteresis loops of UFG pure titanium are basically the same. At a lower total strain amplitude, the hysteresis loop tends to be a straight line. With the increase in total strain amplitude, the size of the hysteresis loop area is increased, which indicates the increase in strain energy consumed during the cyclic process. The energy required for LCF damage is certain. The area of the hysteresis loop represents the work done during the plastic deformation of materials, namely plastic strain energy, which indicates the resistance against the plastic deformation[22]. The area in a hysteresis loop is also a loss of plastic strain energy for each cycle. The larger the plastic strain energy required for the material fatigue damage, the greater the hysteresis loop size, and the shorter the fatigue life.

The hysteresis loop area of UFG pure titanium at half-life cycle under the total strain amplitude of 0.5% is smaller than that of CG pure titanium (Fig. 5b). It infers that UFG pure titanium releases less plastic strain energy at each cycle (19.788 MJ/m^3), compared with CG pure titanium (138.948 MJ/m^3). The higher strength of UFG pure titanium leads to a smaller share of plastic strain and hysteresis loop area under the same total strain amplitude. Therefore, the hysteresis loop area is decreased with the increase in tensile strength. Accordingly, UFG pure titanium has longer LCF life at the

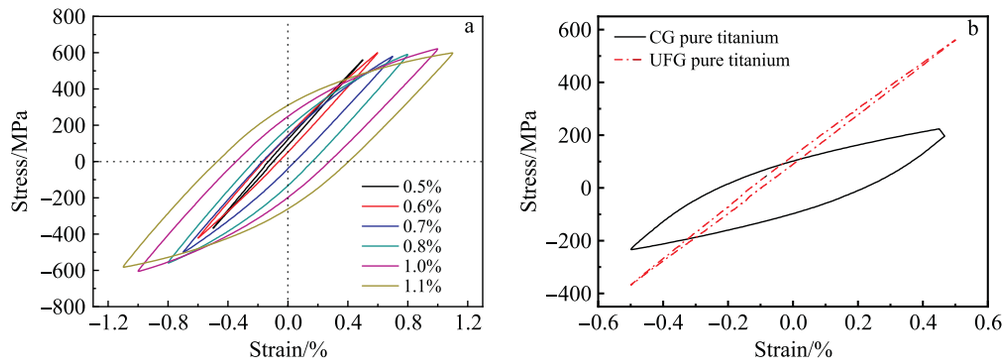

Fig.5 Hysteresis loops of UFG pure titanium at half-life cycle under different total strain amplitudes (a); hysteresis loops of CG and UFG pure titanium at half-life cycle under total strain amplitude of 0.5% (b)

total strain amplitude of 0.5%. To be more specific, at the total strain amplitude of 0.5%, LCF life of UFG pure titanium is 10 850 cycles, and that of CG pure titanium is 4820 cycles. With the decrease in total strain amplitude, the microcrack density is increased, which slows down microcrack propagation and improves the fatigue life (270 cycles at the total strain amplitude of 1.1%).

3.3 LCF life

To analyze the fatigue resistance of UFG pure titanium, a strain-based model that consists of elastic and plastic strains is used. The elastic strain and plastic strain terms are represented by Basquin's equation[23] and Coffin-Manson's equation[24], respectively:

$$\frac{\Delta\varepsilon_e}{2}=\frac{\sigma_f'}{E}(2N_f)^b \tag{2}$$

$$\frac{\Delta\varepsilon_p}{2}=\varepsilon_f'(2N_f)^c \tag{3}$$

where $\frac{\Delta\varepsilon_e}{2}$ is the elastic strain amplitude; σ_f' is the fatigue strength coefficient; E is the elastic modulus; $2N_f$ is the number of reversals to failure; b is the fatigue strength exponent; $\frac{\Delta\varepsilon_p}{2}$ is the plastic strain amplitude; ε_f' is the fatigue ductility coefficient; c is the fatigue ductility exponent. A combination of Eq.(2–3) results in the following equation:

$$\frac{\Delta\varepsilon_t}{2}=\frac{\sigma_f'}{E}(2N_f)^b+\varepsilon_f'(2N_f)^c \tag{4}$$

where $\frac{\Delta\varepsilon_t}{2}$ is the total strain amplitude.

The fatigue parameters (σ_f'/E, ε_f', b, and c) obtained by the data fitting in Eq.(2–3) are listed in Table 2. The relationship curves of the total strain amplitude ($\Delta\varepsilon_t/2$) with reversals to failure ($2N_f$) of UFG and CG pure titanium are plotted in Fig.6.

Table 2 shows the calculated values of fatigue parameters of Coffin-Manson model. It can be seen that UFG pure titanium has higher σ_f' and ε_f', compared with those of CG pure titanium. A high fatigue strength coefficient indicates that the material exhibits greater resistance against plastic deformation during cyclic loading, thereby effectively inhibiting crack initiation and propagation. Additionally, an elevated fatigue ductility coefficient is related to crack-tip plastic deformation, which reflects the crack propagation resistance, significantly decelerating fatigue crack growth. This phenomenon demonstrates that a combination of ECAP and RS achieves synergistic optimization of both parameters, resulting in prolongation of LCF life of UFG pure titanium, particularly at low total strain amplitudes.

Table 2 Fatigue parameters of Coffin-Manson model

Pure titanium	σ_f'/E	b	ε_f'	c
UFG	1.150	−0.082	14.431	−0.563
CG	0.811	−0.125	10.416	−0.430

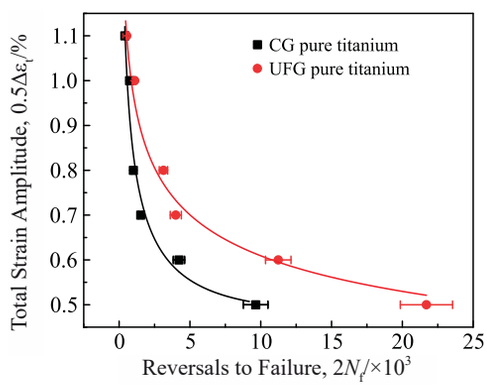

Fig.6 Relationships of $0.5\Delta\varepsilon_t$-$2N_f$ of UFG and CG pure titanium

Coffin et al[25] defines the transition fatigue life N_t, which is the fatigue life corresponding to the plastic strain amplitude equivalent to the elastic strain amplitude (i.e., the intersection points of the curve). Fig.7 shows the relationship between the strain amplitude (plastic and elastic) and the reverse cycle of the load ($2N_f$) of UFG pure titanium. Generally, when N_t is higher than N_f, the contribution of plastic strain to fatigue is greater than that of elastic strain. When N_t is lower than N_f, the elastic strain will play a major role in the fatigue process. It can be seen that the strain fatigue life N_f of UFG pure titanium exceeds the corresponding transition fatigue life N_t under different total strain amplitudes (0.5%–1.1%), which indicates that the transition life for UFG pure titanium is very short. This phenomenon indicates that the fatigue life is more influenced by the fracture strength rather than ductility[26]. In other words, LCF life of UFG pure titanium is similar to that at stress fatigue state. The hindrance of the grain boundary to dislocation slips increases the strength of UFG pure titanium

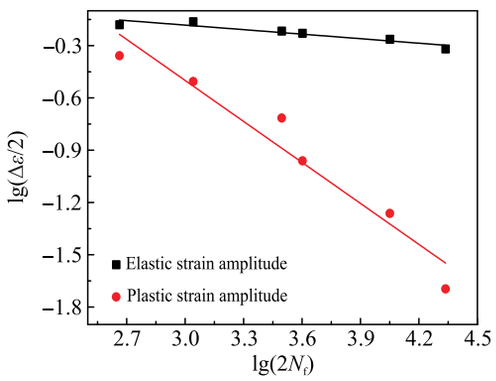

Fig.7 Relationships of $\lg(\Delta\varepsilon/2)$-$\lg(2N_f)$ of UFG pure titanium under elastic and plastic conditions

with higher grain boundary density. Therefore, it is reasonable to interpret that the prolongation of LCF life of UFG pure titanium is mainly attributed to its excellent elastic contribution, i.e., its high tensile strength. UFG pure titanium also has a higher σ_f' (Table 2), which is related to its superior fracture strength in tensile tests. In Ref. [27], Ti2448 alloy possesses good LCF resistance because the recoverable elastic strain mainly endures the applied total cycle strains (4.5%).

3.4 LCF fracture morphology

The fracture surface features of UFG pure titanium after LCF tests at a total strain of 0.5% and 0.8% are shown in Fig. 8 and Fig. 9, respectively. The fatigue fracture can be divided into three typical regions: crack initiation area (Region A), crack propagation area (Region B), and transient breaking area (Region C), as indicated in Fig. 8a and Fig. 9a. The fatigue cracks originate from the specimen surface, presenting the characteristics of multiple crack initiations, which are marked by white arrows. The fatigue crack propagation direction is marked by black arrows in Fig. 8b and Fig. 9b. The fatigue crack propagation regions are characterized by a series of fatigue striations and many microcracks, which are marked by white arrows in Fig. 8c. At higher total strain amplitude (Fig. 9c), there are not only many fatigue striations and microcracks, but also lots of cleavage facets. According to the fracture surface analysis of Fig. 8c and Fig. 9c, microcrack density is reduced with the increase in total strain amplitude. A large microcrack density may result in a shielding effect that can slow down microcrack propagation. Diffuse energy dissipation by (slow) propagation of many cracks may occur, instead of a more localized dissipation by (fast) propagation of a smaller number of cracks[28]. The fracture surface at low strain amplitude presents a higher density of fatigue striations and microcracks, eventually indicating slower crack propagation and a higher resistance against fatigue damage.

At the total strain amplitude of 0.5%, the transient breaking region of UFG pure titanium consists of equiaxed fracture dimples (Fig. 8d), whereas it consists of both equiaxed fracture dimples and cleavage steps at the total strain amplitude of 0.8% (Fig. 9d). Therefore, the fracture morphology exhibits ductile failure and quasi-cleavage failure during cyclic loading with the increase in total strain amplitude, as shown in Fig. 8d

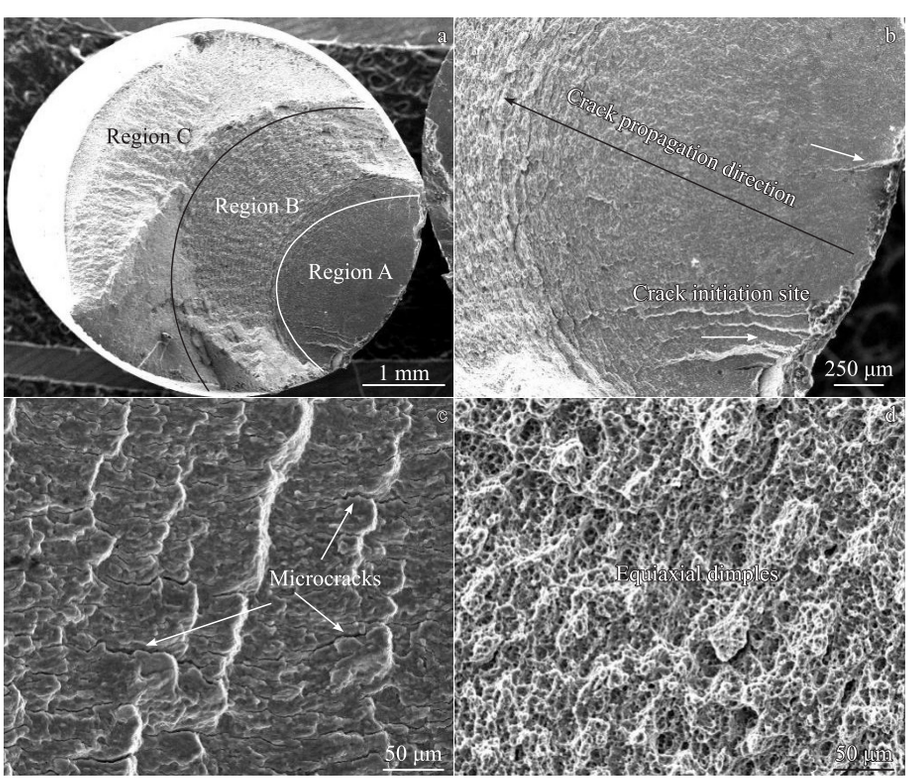

Fig.8 Fatigue fracture morphology of UFG pure titanium at total strain amplitude of 0.5% (a); magnified images of Region A (b), Region B (c), and Region C (d) in Fig.8a

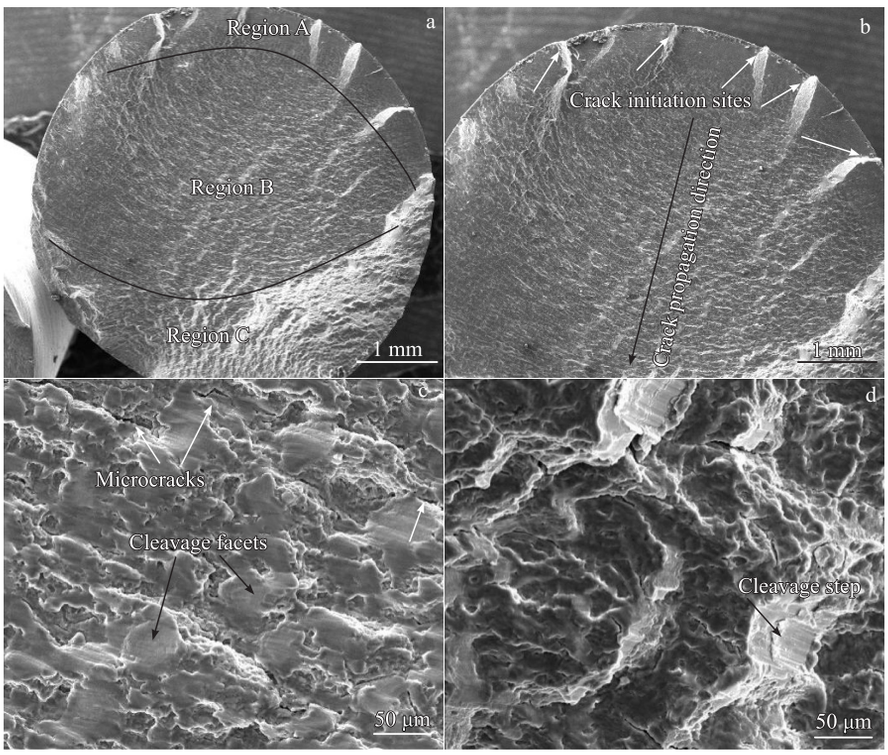

Fig.9 Fatigue fracture morphology of UFG pure titanium at total strain amplitude of 0.8% (a); magnified images of Region A (b), Region B (c), and Region C (d) in Fig.9a

and Fig. 9d, respectively. The released plastic strain energy is less in UFG pure titanium during ductile deformation at low total strain amplitude, whereas quasi-cleavage failure reveals the release of more plastic strain energy during cyclic loading at high total strain amplitude.

3.5 LCF mechanism

Fig. 10 shows the microstructures of UFG pure titanium after fatigue at the total strain amplitude of 0.5% and 1.1%. It can be seen that the microstructures of UFG pure titanium after fatigue depend on the total strain amplitude. No visible changes in the size or shape of grains and the density of dislocations can be observed in the specimen at low total strain amplitude (Fig. 10a and 10c), compared with those in the initial material (Fig. 2b). It means that the microstructure of UFG pure titanium is relatively stable at low total strain amplitude (0.5%). The high fraction of high-angle grain boundaries (HAGBs) in UFG pure titanium also contributes to

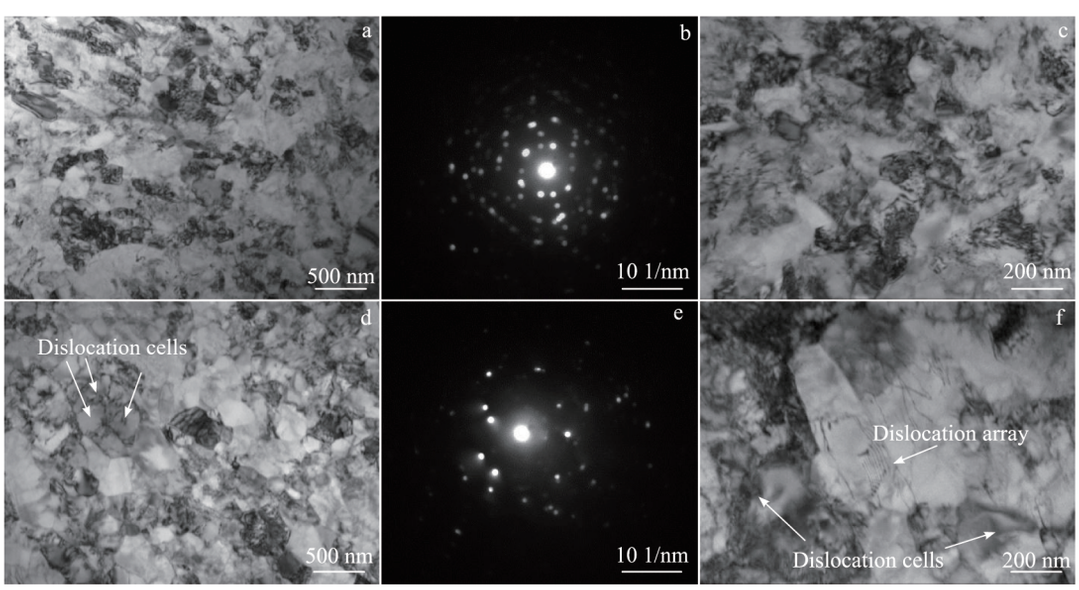

Fig.10 Microstructures (a, c, d, f) and SAED patterns (b, e) of UFG pure titanium after fatigue at total strain amplitude of 0.5% (a–c) and 1.1% (d–f) until failure

its stability (Fig. 10b). However, the microstructure of UFG pure titanium is rather unstable at high strain amplitude (1.1%). It can be seen that the fatigue-induced grain coarsening, dislocation cell formation, and decreased dislocation density occur at high total strain amplitude (1.1%). A clearer planar dislocation array can be observed in the vicinity of grain boundaries, and some grains without dislocations are formed, which are marked by white arrows in Fig. 10f. Compared with SAED pattern in Fig. 10b, the lower fraction of HAGBs probably leads to structure instability (Fig. 10e) at high total strain amplitude. In the process of LCF deformation at room temperature, the rearrangement of dislocations and the dynamic response to elimination make the dislocation entanglement gradually evolve into a large number of dislocation cells. The dislocation density at the cell wall is larger, and the dislocations barely exist in the cell, indicating that the dynamic recovery occurs during LCF deformation of UFG pure titanium (Fig. 10d and 10f). Therefore, LCF mechanisms of UFG pure titanium can be associated with dislocation slip and formation of specific dislocation structures, such as dislocation lines, dislocation tangle, and dislocation cells.

Cyclic hardening and stress saturation appear at the low strain amplitude of 0.5%. The microstructure characteristic of UFG pure titanium after LCF can interpret its cyclic hardening/softening behavior. The cyclic hardening is probably attributed to no visible grain growth or changes in the arrangement or density of dislocations[9], whereas the mechanism of cyclic softening is identified as a complex effect of dislocation recovery, dynamic recrystallization, grain coarsening, and formation of shear bands during the fatigue test[19,29–30]. The softening rate depends strongly on the initial microstructure and loading condition. In this research, the structure stability of UFG pure titanium during LCF is obviously worse than that in other researches on UFG pure titanium, exhibiting pronounced cyclic softening behavior under fatigue loading. This discrepancy may arise from variations in the fabrication techniques employed for the UFG materials. In Ref. [9], UFG pure titanium with the average grain size of 300 nm is produced by ECAP for 8 passes at 400 – 450 °C, resulting in the occurrence of sufficient dynamic recovery and dynamic recrystallization during the processing. However, in this research, UFG pure titanium with the average grain size of 200 nm is produced by ECAP for 4 passes and RS at room temperature. It means that the average dislocation density of UFG pure titanium in Ref. [9] is relatively lower than that in this research. The cyclic softening can be attributed to the existence of a number of dislocations and defects in UFG materials. This result agrees well with the abovementioned TEM observations, which also show pronounced changes in the microstructure (formation of large-sized dislocation cells and grain coarsening) at high strain amplitudes and with higher structure stability (UFGs with HAGBs and high dislocation density) at low strain amplitudes. In other words, the distinct difference between hardening and softening responses at different total strain amplitudes is due to different stress levels, i. e., a more substantial annihilation and rearrangement of the dislocations promoted by very high external stress at a total strain amplitude of 1.1%.

4 Conclusions

1) The strain-controlled LCF life of UFG pure titanium is improved in the applied total strain amplitude of 1.1%, compared with that of CG pure titanium, which is attributed to high tensile strength, resulting in a small hysteresis loop area (less fatigue damage).

2) Cyclic hardening and stress saturation appear at the low strain amplitude of 0.5%, whereas cyclic softening occurs at all other total strain amplitudes, which is attributed to the better structure stability at low strain amplitudes and the formation of large-sized dislocation cells and grain coarsening at high strain amplitudes.

3) The fatigue fracture surface of UFG pure titanium exhibits obvious fatigue striations and microcracks. With the decrease in total strain amplitude, the microcrack density is increased, which slows down microcrack propagation and improves the fatigue life (270 cycles at the total strain amplitude of 1.1%; 10 850 cycles at the total strain amplitude of 0.5%).

References

1 Han X, Ma J X, Tian A X *et al*. *Colloids and Surfaces B: Biointerfaces*[J], 2023, 227: 113339

2 Song B, Ma C L, Xi H L *et al*. *Rare Metal Materials and Engineering*[J], 2024, 53(11): 3001

3 Zhao Q Y, Sun Q Y, Xin S W *et al*. *Materials Science & Engineering A*[J], 2022, 845: 143260

4 Qiang M, Yang X R, Liu X Y *et al*. *Rare Metal Materials and Engineering*[J], 2023, 52(5): 1673

5 Tesař K, Koller M, Vokoun D *et al*. *Materials & Design*[J], 2023, 226: 111678

6 Yang X R, Wang Z L, Dai Y *et al*. *Journal of Materials Research and Technology*[J], 2024, 28(23): 3976

7 Höppel H W, Kautz M, Xu C *et al*. *International Journal of Fatigue*[J], 2006, 28(9): 1001

8 Saitova L R, Höppel H W, Göken M *et al*. *Materials Science & Engineering A*[J], 2009, 503: 145

9 Vinogradov A Y, Stolyarov V V, Hashimoto S *et al*. *Materials Science & Engineering A*[J], 2001, 318(1–2): 163

10 Hockauf K, Wagner M F X, Halle T *et al*. *Acta Materialia*[J], 2014, 80: 250

11 Meng L, Anchal G, Véronique D. *International Journal of Fatigue*[J], 2019, 121: 84

12 Sreearravind M, Ravisankar B, Ramesh K S. *Materials Today Communications*[J], 2025, 42: 111401

13 Vinogradov A, Hashimoto S, Kopylov V I. *Materials Science &*

Engineering A[J], 2003, 355(1–2): 277
14 Yang X R, Zhang W Y, Liu X Y *et al*. *Rare Metal Materials and Engineering*[J], 2019, 48(4): 1202
15 Alexander V P, Georgy I R, Irina P S *et al*. *Materials Letters*[J], 2021, 302: 130366
16 Figueiredo R B, De Barbosa E R C, Zhao X C *et al*. *Materials Science & Engineering A*[J], 2014, 619: 312
17 Naseri R, Hiradfar H, Shariati M *et al*. *Archives of Civil & Mechanical Engineering*[J], 2018, 18(3): 755
18 Semenova I P, Salimgareeva G K, LatyshSaitova V V *et al*. *Materials Science & Engineering A*[J], 2009, 503(1–2): 92
19 Gabor P, Karaman I. *Materials Science & Engineering A*[J], 2005, 410–411: 457
20 Wu Y J, Zhu R. *Material Reports B*[J], 2013, 27(11): 104
21 Hill N, Mather D, Stafford H. *Annual Book of ASTM Standards*[M]. Philadelphia: ASTM, 1996
22 Suresh S. *Fatigue of Materials*[M]. Cambridge: Cambridge University Press, 1998
23 Basquin O H. *Proceedings: American Society for Testing and Materials*[J], 1910, 10: 625
24 Coffin L F. *Journal of Fluids Engineering*[J], 1954, 76(8): 931
25 Coffin L F. *Advances in Research on the Strength & Fracture of Materials*[M]. New York: Elsevier, 1978: 263
26 Cantó J S, Winwood S, Rhodes K *et al*. *Materials Science & Engineering A*[J], 2018, 718: 19
27 Zhang S Q, Li S J, Jia M T *et al*. *Acta Materialia*[J], 2011, 59(11): 4690
28 Li M, Goyal A, Doquet V *et al*. *International Journal of Fatigue*[J], 2019, 121: 84
29 Zhang Z J, Zhang P, Zhang Z F. *Acta Materialia*[J], 2016, 121: 331
30 Mughrabi H, Höppel H W. *International Journal of Fatigue*[J], 2010, 32(9): 1413

超细晶纯钛的低周疲劳行为

刘晓燕，王子轩，杨西荣，罗　雷，王敬忠
(西安建筑科技大学 冶金工程学院，陕西 西安 710055)

摘　要：采用室温4道次等径弯曲通道变形+旋锻制备超细晶纯钛，利用Instron型电液伺服疲劳试验机在室温下分别对粗晶和超细晶纯钛进行应变控制的低周疲劳试验，应变幅范围为0.5%~1.1%。通过透射电子显微镜和扫描电子显微镜研究超细晶纯钛疲劳变形后的组织和断口形貌。结果表明：与粗晶纯钛相比较，超细晶纯钛具有更高的低周疲劳寿命，例如在总应变幅为0.5%时，超细晶和粗晶纯钛的疲劳寿命分别为10 850和4820周次。除总应变幅为0.5%外，超细晶纯钛在疲劳变形过程中表现出显著的循环软化现象。随着总应变幅的增大，疲劳滞后回线所包含的面积增大。断口形貌显示疲劳裂纹萌生于试样表面，疲劳扩展区存在大量疲劳辉纹和微裂纹，随着应变幅的增加，疲劳断裂模式由韧性断裂转变为准解理断裂。超细晶纯钛低周疲劳变形机理为位错滑移。

关键词：超细晶纯钛；等径弯曲通道变形+旋锻；低周疲劳；位错滑移

作者简介：刘晓燕，女，1980年生，博士，副教授，西安建筑科技大学冶金工程学院，陕西 西安 710055，E-mail：liuxiaoyan@xauat.edu.cn